Pharmaceutical Sciences and Drug Design
ISSN: 3062-4428
2025, Volume 5, Page No: 152-166

Available online at: www.galaxypub.co/page/journals

Galaxy Publication

Correlative Analysis of Gut Microbiota and Metabolic Profiles in Methotrexate-Induced Hepatotoxic Mice through Integrated Microbiome and Metabolome Study

Nicole Baker[1]*, Paige Stewart[1]

[1]Department of Phytochemistry, Faculty of Pharmacy, University of Alberta, Edmonton, Canada.

***E-mail** ✉ nicole.baker.ca@gmail.com

Received: 12 April 2025; **Revised:** 18 August 2025; **Accepted:** 21 August 2025

ABSTRACT

This study aimed to explore potential relationships between gut microbiota composition and hepatic metabolic disturbances in mice with methotrexate (MTX)-induced hepatotoxicity.Hepatotoxicity was induced in healthy Kunming mice using MTX, followed by measurements of plasma ALT and AST levels and histopathological examination of liver tissue. An integrated approach combining gas chromatography–mass spectrometry (GC-MS) and 16S rRNA gene sequencing was employed to assess MTX-induced alterations in gut microbiota and liver metabolic profiles. Spearman correlation analysis was used to identify associations between gut microbial changes and hepatic metabolomic profiles.MTX administration led to elevated ALT and AST levels and evident liver damage. MTX disrupted multiple metabolic pathways, including amino acid biosynthesis (valine, leucine, isoleucine, arginine) and metabolism (alanine, aspartate, glutamate, histidine, beta-alanine, glycine, serine, threonine), aminoacyl-tRNA biosynthesis, pantothenate and CoA biosynthesis, as well as energy, glutathione, porphyrin, and chlorophyll metabolism. Gut microbiota analysis revealed increases in Staphylococcus, Enterococcus, Collinsella, Streptococcus, and Aerococcus, alongside decreases in Lactobacillus, Ruminococcus, norank_f_Muribaculaceae, unclassified_f_Lachnospiraceae, norank_f_Lachnospiraceae, A2, Eubacterium_xylanophilum_group, Phascolarctobacterium, Bifidobacterium, and Faecalibaculum. Correlation analysis indicated that shifts in the abundance of Phascolarctobacterium, Faecalibaculum, norank_f_Muribaculaceae, Streptococcus, Enterococcus, Staphylococcus, and Collinsella were associated with liver injury.The findings suggest that MTX-induced hepatotoxicity is closely linked to alterations in gut microbiota composition and hepatic metabolite profiles, highlighting potential strategies for mitigating MTX-related liver damage.

Keywords: Hepatoxicity, Gas chromatography-mass spectrometry, Methotrexate, 16S Ribosomal RNA

How to Cite This Article: Baker N, Stewart P. Correlative Analysis of Gut Microbiota and Metabolic Profiles in Methotrexate-Induced Hepatotoxic Mice through Integrated Microbiome and Metabolome Study. Pharm Sci Drug Des. 2025;5:152-66. https://doi.org/10.51847/Q6Vr9aHuB4

Introduction

Methotrexate (MTX), a folate antagonist and antimetabolite, is widely used in treating pediatric acute leukemia and is a common chemotherapeutic agent for cancers such as hepatocellular carcinoma, breast, lung, and gastric cancers [1]. Beyond oncology, MTX serves as an immunosuppressive therapy for autoimmune disorders, including systemic connective tissue diseases, psoriasis, systemic lupus erythematosus, inflammatory bowel disease, sicca syndrome, and rheumatoid arthritis [2]. While gastrointestinal side effects such as nausea, vomiting, diarrhea, abdominal discomfort, constipation, pancreatitis, or small-bowel obstruction are frequently reported [3], hepatotoxicity remains the most clinically significant adverse effect [4]. Elevated liver transaminases are commonly observed post-MTX treatment, often accompanied by histological alterations in the liver. For instance, in rheumatoid arthritis patients receiving MTX, mild liver fibrosis occurred in 15.3%, severe fibrosis in 1.3%, and cirrhosis in 0.5% of cases [5]. Despite these findings, the precise mechanisms of MTX-induced hepatotoxicity are not fully understood.

The gut microbiota, referred to as “a virtual metabolic organ,” significantly influences extraintestinal organs, including the liver, kidneys, brain, and cardiovascular and skeletal systems [6–8]. Disruptions in gut microbial communities have been linked to various liver disorders [9]. The liver and gut are connected through the gut-liver axis via the portal vein, biliary tract, and systemic circulation. Compromised intestinal barriers increase gut permeability, enabling translocation of microbes to the liver and altering its function [10]. Conversely, the liver affects the gut by secreting bile acids and bioactive compounds into the biliary system and circulation [10]. Specific hepatic metabolites, such as inosine, taurine, glutathione, aminohydroxybutyric acid, cholic acid, and L-lysine, correlate with gut microbiota abundance, highlighting crosstalk between hepatic metabolism and microbial composition during liver injury, including acute alcohol-induced damage [11]. Although MTX hepatotoxicity has been examined [12], the link between MTX-induced gut microbiota changes and liver injury remains largely unexplored. We hypothesize that alterations in gut microbiota composition are associated with MTX-driven changes in hepatic metabolism.

Integrated approaches combining metabolomics and 16S rRNA gene sequencing have emerged as effective tools to investigate gut microbiota composition and its influence on metabolic or functional phenotypes in disease contexts [13, 14]. These strategies also facilitate the identification of gut microbiota-mediated effects of drugs, including both therapeutic and toxic outcomes [15, 16]. Accordingly, this study applied GC-MS-based metabolomics in combination with 16S rRNA sequencing to examine interactions between gut microbiota and hepatic metabolic pathways in MTX-treated mice. Our work aims to elucidate the mechanisms underlying MTX-induced hepatotoxicity and provide a foundation for potential therapeutic interventions.

Materials and Methods

Chemicals and reagents

MTX (99% purity), heptadecanoic acid (≥98%), methanol (chromatographic grade), and pyridine were obtained from Macklin Biochemical (Shanghai, China). O-methylhydroxylamine hydrochloride (≥98%) was purchased from J&K Scientific (Beijing, China), and N,O-bis(trimethylsilyl) trifluoroacetamide containing 1% trimethylchlorosilane (BSTFA+1% TMCS) was obtained from Sigma Aldrich (St. Louis, MO, USA). Purified water was sourced from Wahaha (Hangzhou, China). All experiments followed institutional animal care guidelines and were approved by the Ethical Committee for Animal Experimentation of the Affiliated Hospital of Jining Medical University (approval number: 2022B070).

Animal models and treatment protocol

Fourteen male Kunming mice (5 weeks old, 30–35 g) were purchased from Pengyue Experimental Animal Breeding (Jinan, China; approval number: SCXK20190003) and housed under controlled conditions (20 ± 2 °C, 65% humidity, 12 h light/dark cycle) with unrestricted access to food and water. After a 7-day acclimation, mice were randomly assigned to either the MTX group or control group (seven per group). MTX-treated mice received daily intraperitoneal injections of MTX (5 mg/kg) for 7 days, with the volume adjusted according to body weight (0.1 mL/10 g). Controls received equivalent volumes of saline. The MTX dose was adapted from previous studies with minor adjustments [17].

Sample collection

Following the treatment period, mice were anesthetized with 1% sodium pentobarbital (50 mg/kg), and blood was collected via ocular extraction. Serum was separated by centrifugation at 4000 rpm for 10 min at 4 °C and stored at −80 °C. Mice were euthanized via cervical dislocation; livers and colons were excised, washed with PBS, frozen in liquid nitrogen, and stored at −80 °C.

Liver sample preparation for metabolomics

Liver tissues (50 mg) were homogenized in 1 mL methanol, spiked with 50 µL heptadecanoic acid (1 mg/mL), and centrifuged at 14,000 rpm for 15 min at 4 °C. Supernatants were derivatized with 80 µL O-methylhydroxylamine hydrochloride (15 mg/mL in pyridine) at 70 °C for 90 min, followed by 100 µL BSTFA+1% TMCS at 70 °C for 60 min. Samples were filtered through 0.22 µm filters. Quality control (QC) samples were prepared by pooling 10 µL from each sample within the same group.

Assessment of hepatotoxicity

Serum ALT and AST levels were quantified using commercial assay kits (Jiancheng Bioengineering Institute, Nanjing, China) according to manufacturer instructions (UNICO Instruments, Model 1200, USA).

Histopathology

Liver samples were dehydrated in ethanol and xylene, embedded in paraffin, sectioned at 5 μm, and stained with hematoxylin and eosin (H&E). Slides were scanned using a 3D panoramic scanner (HISTECH Panoramic 250, Hungary) to identify histopathological changes.

GC-MS metabolomics analysis

Metabolomic profiling was performed using an Agilent 7890B GC system coupled to a 7000C mass spectrometer (Agilent Technologies, USA) with an HP-5MS fused silica column. One microliter of each sample was injected at a 50:1 split ratio. Helium served as the carrier gas at 1 mL/min. Temperatures were set as follows: injection 280 °C, transfer line 250 °C, ion source 230 °C. Electron impact ionization was applied at −70 eV, with acquisition at 20 spectra/s, and scanning over m/z 50–800.

Data processing and multivariate analysis

Raw GC-MS data were processed using Agilent Mass Hunter (Version B.07.00, Agilent Technologies, CA, USA). Preprocessing steps included retention time alignment, baseline correction, deconvolution, and filtering. To identify metabolites, a spectral library was built from all QC samples, and unknown compounds were matched against the NIST 14 GC-MS library. Metabolites with a similarity score above 80% were considered reliably identified, and all identifications were manually checked to minimize errors from automated deconvolution and eliminate false positives. Using these verified spectra, a custom “New Library” was created for matching experimental sample spectra.

An integrated data matrix was constructed containing the peak index (RT–m/z), sample identifiers, and normalized peak areas using Microsoft Excel™ (Microsoft, Redmond, WA, USA). Further multivariate analyses were performed in SIMCA-P 14.0 (Umetrics, Sartorius Stedim Biotech), including principal component analysis (PCA) and orthogonal partial least squares discriminant analysis (OPLS-DA). Group comparisons were conducted using two-tailed Student’s t-tests. Compounds with VIP values > 1.0 and p-values < 0.05 were considered potential differential metabolites. These metabolites were further visualized via heatmaps and pathway enrichment analyses using MetaboAnalyst 5.0 (http://www.metaboanalyst.ca).

16S rRNA sequencing of gut microbiota

Gut microbial communities were profiled by 16S rRNA gene sequencing through Majorbio Bio-Pharm Technology (Shanghai, China). Genomic DNA was extracted from colonic contents using the E.Z.N.A.® Soil DNA Kit (Omega Bio-tek, Norcross, GA, USA), and DNA integrity was confirmed by 1% agarose gel electrophoresis. The V3–V4 hypervariable regions of the bacterial 16S rRNA gene were amplified using TransStart FastPfu DNA Polymerase (TransGen AP221-02) on a GeneAmp 9700 PCR system (ABI, USA). PCR products were purified and sequenced on the Illumina MiSeq platform (Illumina, USA) using the TruSeqTM DNA Sample Prep Kit. Raw reads were processed following the RS_ReadsOfinsert1 protocol.

High-quality sequences were filtered using QIIME (Version 1.9.1, http://qiime.org/install/index.html), and OTU clustering was performed with UPARSE (Version 7.1) at a 97% similarity threshold, with chimeric sequences removed. Taxonomic classification was conducted using the Ribosomal Database Project (RDP) Bayesian classifier against the Silva 16S rRNA database at a 70% confidence threshold. Alpha and beta diversity metrics, as well as community composition analyses, were performed. Functional predictions for microbial communities were made using PICRUSt2 (Version 1.1.0, http://picrust.github.io/picrust/) with COG annotation. Spearman correlation analysis was conducted to explore associations between gut microbiota abundances and hepatic metabolite levels, visualized as a heatmap.

Results and Discussion

MTX-induced hepatotoxicity in mice

Mice treated with MTX exhibited significant increases in serum ALT and AST compared to controls (**Figures 1a and 1b**; $p < 0.001$). Histological examination of control livers revealed normal hepatocyte architecture with no detectable abnormalities **(Figure 1c)**. In contrast, liver sections from MTX-treated mice showed pathological changes, including uneven cytoplasmic staining, nuclear aggregation of nucleoli, cytoplasmic swelling, and loosening. Connective tissue proliferation and inflammatory cell infiltration were also evident **(Figure 1d)**, confirming that MTX induced hepatotoxicity in this mouse model.

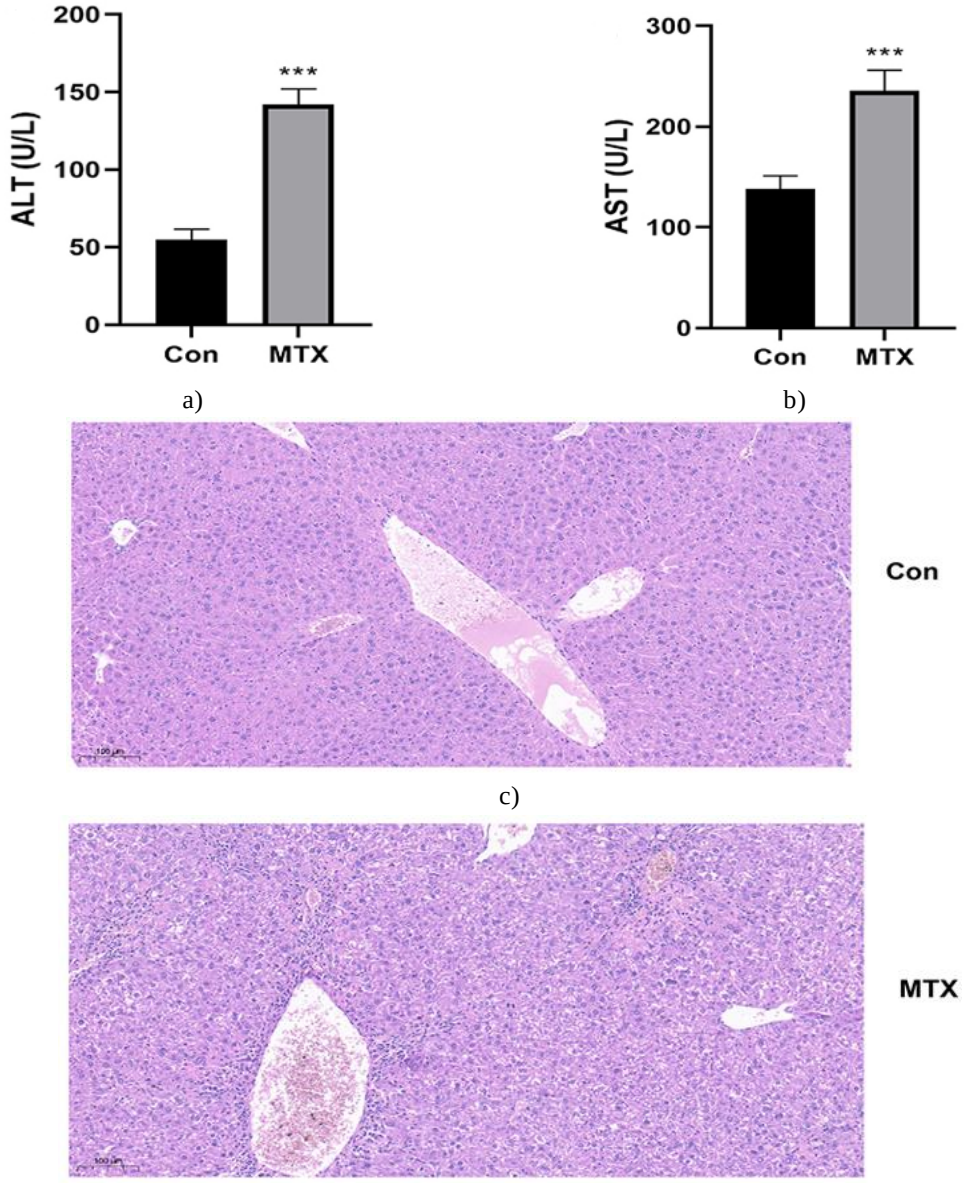

Figure 1. MTX-induced hepatotoxicity in mice. (a) Serum ALT and (b) AST levels in MTX-treated and control mice. Representative H&E-stained liver sections showing (c) normal hepatocyte morphology in controls and (d) pathological changes in MTX-treated mice. ***$p < 0.001$ vs. control group.

Hepatic metabolomic alterations in MTX-Treated mice by GC-MS

To evaluate the impact of MTX on liver metabolism, an untargeted GC-MS-based metabolomics approach was employed. Total ion chromatograms (TICs) for QC, control, and MTX liver samples are presented in **Figures 2a–2c**. Multivariate analyses, including PCA and OPLS-DA, revealed distinct separation between the MTX and control groups **(Figures 3a and 3b)**. Permutation testing with 200 iterations confirmed the robustness and predictive accuracy of the OPLS-DA model, with $R^2Y = 1.0$ and $Q^2Y = 0.959$ **(Figure 3c)**, indicating reliable differentiation between the two experimental conditions.

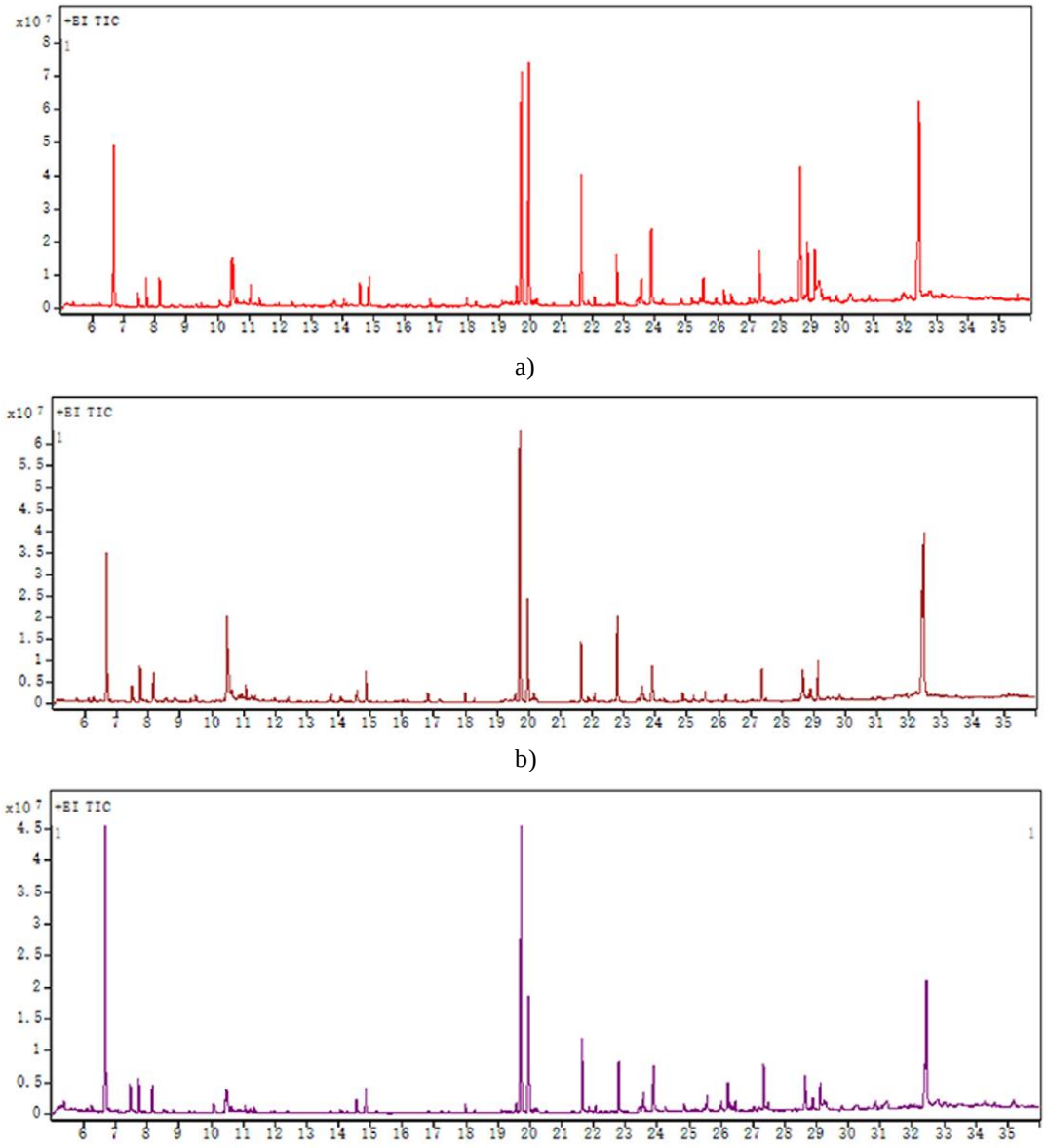

Figure 2. Representative GC-MS Total Ion Chromatograms (TICs) of Mouse Liver Samples. (a) Quality control (QC) sample, (b) control group sample, and (c) MTX-treated group sample.

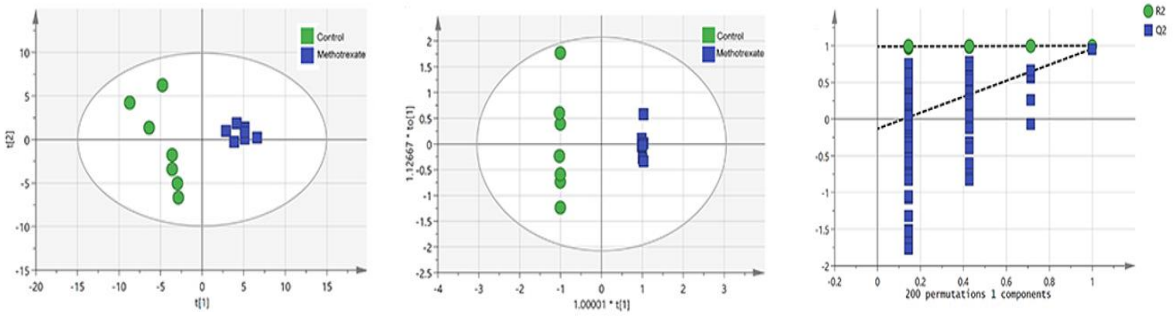

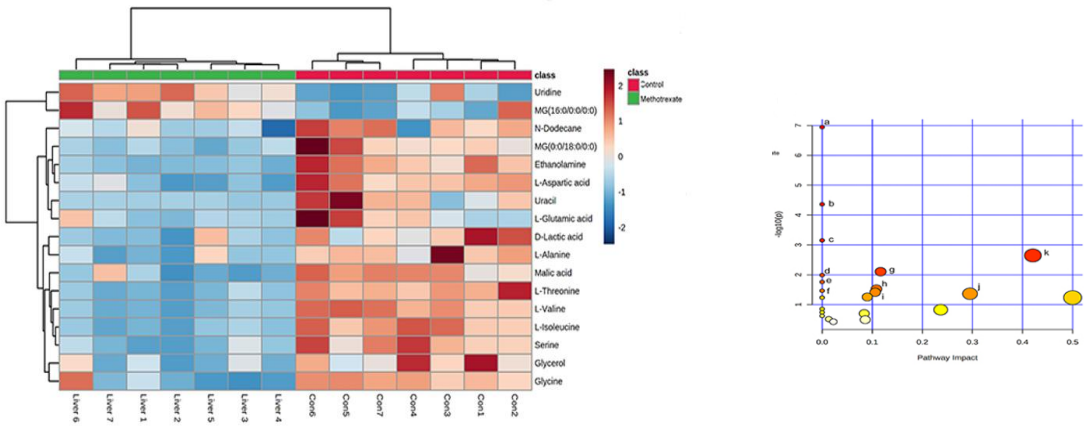

d) e)

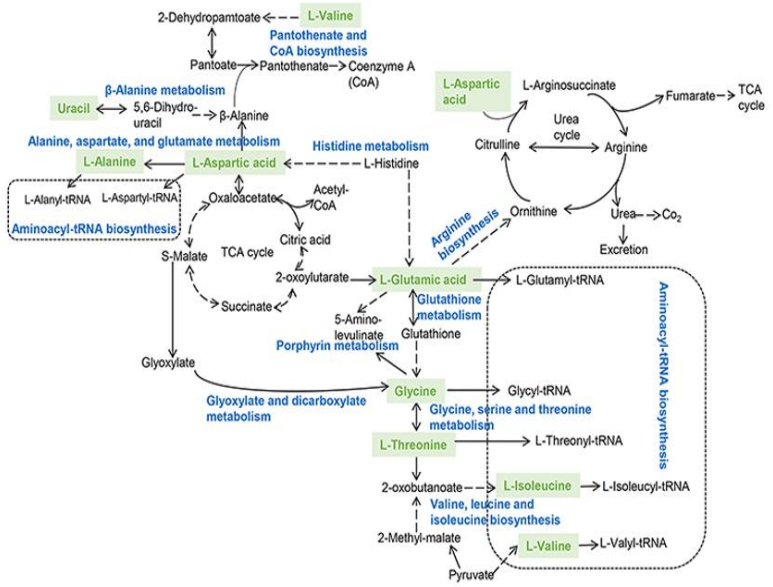

f)

Figure 3. MTX-Induced alterations in hepatic metabolomic profiles of mice. (a) PCA score plot showing separation between control and MTX-treated groups. (b) OPLS-DA score plot differentiating control and MTX groups ($R^2Y = 1.0$, $Q^2Y = 0.959$). (c) Validation of the OPLS-DA model through 200 permutation tests. (d) Heatmap illustrating relative levels of metabolites with VIP > 1.0 and $p < 0.05$. (e) Summary of metabolic pathways significantly impacted by MTX ($p < 0.05$); a: aminoacyl-tRNA biosynthesis, b: valine, leucine, and isoleucine biosynthesis, c: pantothenate and CoA biosynthesis, d: histidine metabolism, e: beta-alanine metabolism, f: porphyrin and chlorophyll metabolism, g: arginine biosynthesis, h: glutathione metabolism, i: glyoxylate and dicarboxylate metabolism, j: glycine, serine, and threonine metabolism, k: alanine, aspartate, and glutamate metabolism. (f) Schematic representation of hepatic metabolic pathways altered by MTX; green labels indicate downregulated metabolites in MTX-treated mice.

Metabolites with VIP > 1 in OPLS-DA and $p < 0.05$ in Student's t-tests were considered potential biomarkers distinguishing the two groups. Cluster analysis **(Figure 3d)** revealed that uridine and 1-monopalmitin (MG(16:0/0:0/0:0)) were elevated, whereas several amino acids, D-lactic acid, malic acid, N-dodecane, ethanolamine, glycerol, uracil, and glycerol monostearate (MG(0:0/18:0/0:0)) were reduced following MTX treatment. Pathway enrichment analysis demonstrated that MTX primarily disrupted amino acid metabolism and biosynthesis, aminoacyl-tRNA biosynthesis, pantothenate and CoA biosynthesis, glutathione metabolism, porphyrin and chlorophyll metabolism, as well as glyoxylate and dicarboxylate metabolism **(Table 2; Figures 3e and 3f)**.

Table 1. Differentially-expressed metabolites in the liver of mice after MTX challenge

Metabolites	HMDB	KEGG	VIP	*p*-value	Fold Change
D-Lactic acid	HMDB0001311	C00256	1.091	0.002	0.537
L-Valine	HMDB0000883	C00183	1.789	0.000	0.231
L-Alanine	HMDB0000161	C00041	1.395	0.001	0.371
N-Dodecane	HMDB0031444	C08374	1.135	0.003	0.476
Ethanolamine	HMDB0000149	C00189	1.764	0.000	0.229
Glycerol	HMDB0000131	C00116	1.122	0.001	0.556
L-Isoleucine	HMDB0000172	C00407	1.776	0.000	0.241
Glycine	HMDB0000123	C00037	1.394	0.004	0.398
Uracil	HMDB0000300	C00106	1.638	0.005	0.163
Serine	HMDB0062263	C00716	1.226	0.004	0.461
L-Threonine	HMDB0000167	C00188	1.503	0.000	0.379
L-Aspartic acid	HMDB0000191	C00049	1.527	0.000	0.350
Malic acid	HMDB0000744	C03668	1.328	0.001	0.455
L-Glutamic acid	HMDB0000148	C00025	1.242	0.012	0.375
Uridine	HMDB0000296	C00299	1.157	0.002	2.159
MG (16:0/0:0/0:0)	HMDB0011564	-	1.266	0.003	2.637
MG (0:0/18:0/0:0)	HMDB0011535	-	1.575	0.000	0.278

Abbreviations: HMDB, Human Metabolome Database; VIP, variable influence on projection.

Table 2. Pathway analysis results obtained from metaboanalyst 5.0

Pathway Name	Raw *p*	-log(*p*)	Impact
Aminoacyl-tRNA biosynthesis	1.14E-07	6.9449	0
Valine, leucine, and isoleucine biosynthesis	4.35E-05	4.3613	0
Pantothenate and CoA biosynthesis	7.05E-04	3.1519	0
Alanine, aspartate, and glutamate metabolism	0.0022573	2.6464	0.42068
Arginine biosynthesis	0.0078672	2.1042	0.11675
Histidine metabolism	0.010255	1.989	0
Beta-Alanine metabolism	0.017438	1.7585	0
Glutathione metabolism	0.03015	1.5207	0.10839
Porphyrin metabolism	0.034301	1.4647	0
Glyoxylate and dicarboxylate metabolism	0.038665	1.4127	0.10582
Glycine, serine, and threonine metabolism	0.043233	1.3642	0.29525

MTX-induced alterations in gut microbiota

High-throughput 16S rRNA sequencing was performed to assess the effects of MTX on gut microbial populations. Analysis of alpha diversity revealed that MTX treatment altered microbial richness and diversity, as reflected by the Chao1 and Ace indices **(Figures 4a and 4b)**. Good's coverage indicated that the sequencing depth adequately captured the gut microbiome composition **(Figure 4c).** Beta diversity, evaluated using principal coordinate analysis (PCoA) based on Bray-Curtis distances, demonstrated clear segregation between the control and MTX groups at the OTU level, indicating that MTX significantly reshaped the gut microbial community structure **(Figure 4d).**

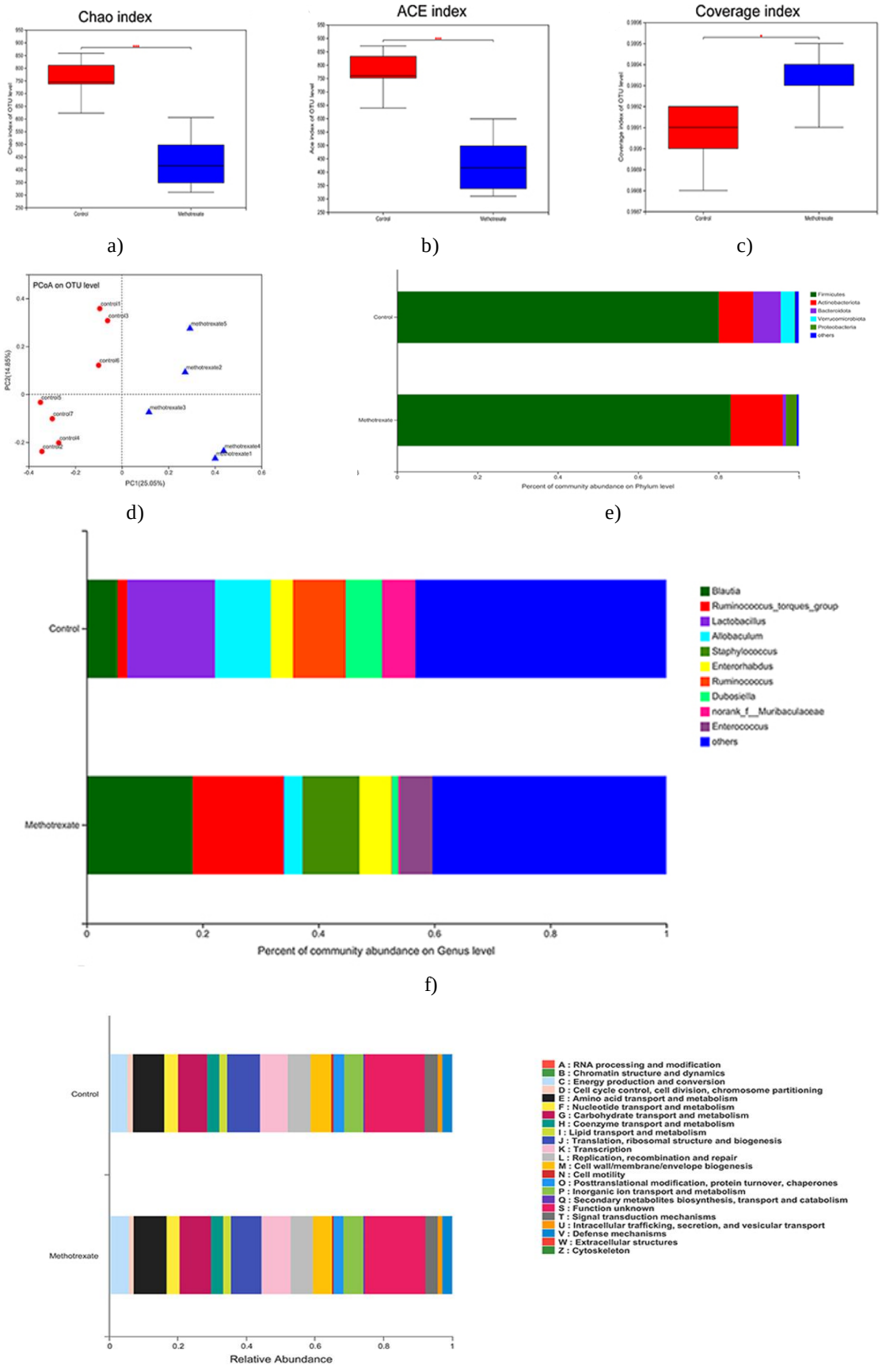

Figure 4. Alterations in gut microbiota following MTX administration. Alpha-diversity metrics were evaluated using the Chao1, Ace, and Good's coverage indexes **(Figures 4a–4c)**, and OTU-level differences

were visualized with a PCoA score plot **(Figure 4d)**. Microbial composition was examined at both the phylum **(Figure 4e)** and genus levels **(Figure 4f)**, and predicted functional profiles were inferred via PICRUSt COG classification **(Figure 4g)**. Statistical significance is denoted as *p < 0.05 and ***p < 0.001 relative to controls.

At the phylum level, the control mice gut microbiota was dominated by Firmicutes (80.11%), Actinobacteriota (8.58%), Bacteroidota (6.84%), Verrucomicrobiota (3.47%), and Proteobacteria (0.08%). In contrast, MTX treatment led to higher proportions of Firmicutes (83.02%), Actinobacteriota (13.00%), and Proteobacteria (2.69%), while Bacteroidota (0.78%) and Verrucomicrobiota (0.00%) were reduced **(Figure 4e)**. At the genus level, pre-MTX samples were mainly composed of Lactobacillus (15.14%), Allobaculum (9.62%), Ruminococcus (9.10%), Dubosiella (6.26%), norank_f_Muribaculaceae (5.73%), Blautia (5.35%), Enterorhabdus (3.84%), Ruminococcus_torques_group (1.68%), and Enterococcus (0.01%). Following MTX exposure, the relative abundances of Blautia (18.32%), Ruminococcus_torques_group (15.63%), Staphylococcus (9.83%), Enterorhabdus (5.55%), and Enterococcus (5.54%) increased, whereas Lactobacillus (0.14%), Allobaculum (3.16%), norank_f_Muribaculaceae (0.31%), Dubosiella (1.12%), and Ruminococcus (0.07%) declined **(Figure 4f)**. Functional analysis via COG prediction revealed that MTX administration elevated the representation of categories related to energy production and conversion, amino acid transport and metabolism, carbohydrate transport and metabolism, transcription, coenzyme transport and metabolism, and inorganic ion transport and metabolism **(Figure 4g).**

For microbial population comparisons **(Figure 5)**, the Firmicutes/Bacteroidota (F/B) ratio increased dramatically in MTX-treated mice (106.64) relative to controls (11.72) **(Figure 5a)**. Wilcoxon rank-sum testing identified significant shifts in taxonomic composition between the groups. At the phylum level, MTX exposure reduced Bacteroidota ($p < 0.01$), unclassified_k_norank_d_Bacteria ($p < 0.01$), and Fusobacteriota ($p < 0.05$), while Deferribacterota increased ($p < 0.05$) compared with controls **(Figure 5b)**. At the genus level, MTX-treated mice displayed significant decreases in Lactobacillus ($p < 0.01$), Ruminococcus ($p < 0.01$), norank_f_Muribaculaceae ($p < 0.01$), unclassified_f_Lachnospiraceae ($p < 0.05$), norank_f_Lachnospiraceae ($p < 0.05$), A2 ($p < 0.01$), Eubacterium_xylanophilum_group ($p < 0.05$), Phascolarctobacterium ($p < 0.05$), Bifidobacterium ($p < 0.05$), and Faecalibaculum ($p < 0.01$), while Staphylococcus ($p < 0.05$), Enterococcus ($p < 0.01$), Collinsella ($p < 0.05$), Streptococcus ($p < 0.05$), and Aerococcus ($p < 0.05$) were markedly enriched compared to controls **(Figure 5c).**

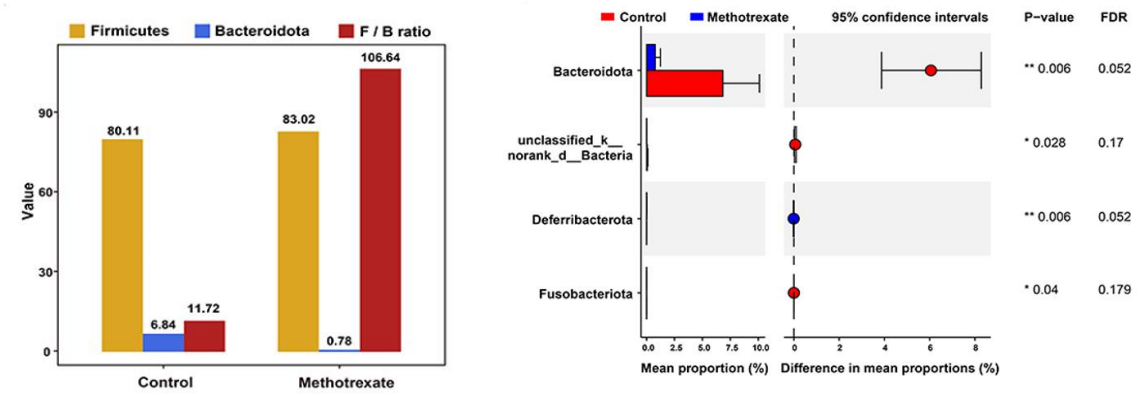

a) b)

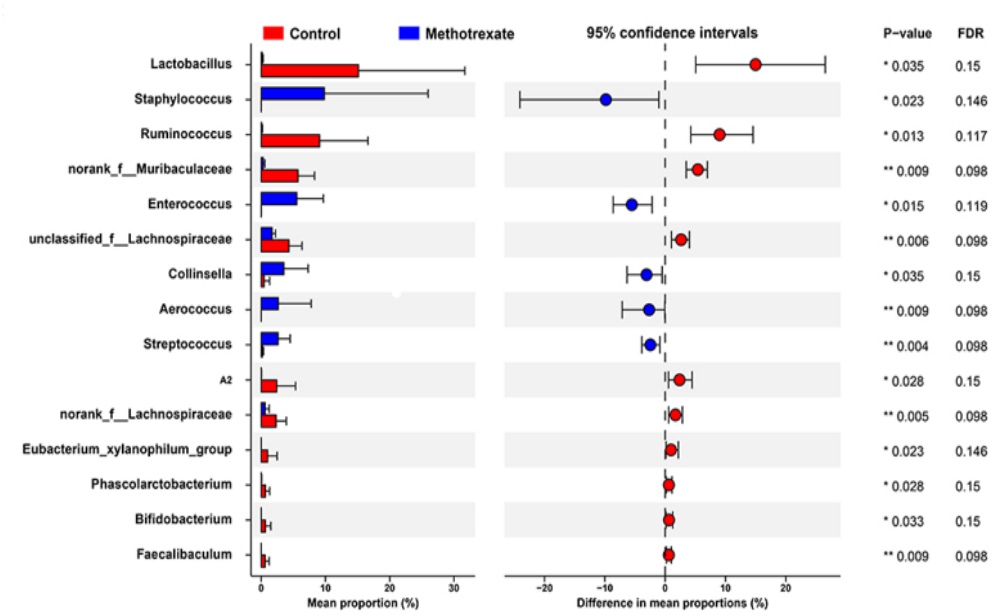

c)

Figure 5. F/B ratio in control and MTX-treated mice **(Figure 5a)**, along with Wilcoxon rank-sum test comparisons of microbial populations at the (b) phylum and (c) genus levels. Statistically significant differences between the groups are indicated as *p < 0.05 and **p < 0.01.

Correlation analysis between hepatic metabolic biomarkers and gut microbiota

To explore relationships between gut microbiota and liver metabolites, Spearman correlation analysis was performed at the genus level. Several bacterial genera, including Phascolarctobacterium, Faecalibaculum, Aerococcus, A2, Streptococcus, norank_f_Muribaculaceae, Enterococcus, Staphylococcus, Collinsella, Ruminococcus, and Lactobacillus, exhibited strong correlations with multiple metabolites (correlation coefficient > 0.5 or < −0.5). As shown in **Figure 6**, Phascolarctobacterium, Faecalibaculum, A2, norank_f_Muribaculaceae, Ruminococcus, and Lactobacillus were positively associated with L-valine, ethanolamine, glycine, serine, L-threonine, and L-aspartic acid. Additionally, Phascolarctobacterium, Faecalibaculum, norank_f_Muribaculaceae, and Ruminococcus displayed positive correlations with uracil but negative correlations with uridine. A2, norank_f_Muribaculaceae, and Lactobacillus were all positively linked to L-alanine and L-glutamic acid, while Lactobacillus also showed a positive association with D-lactic acid.

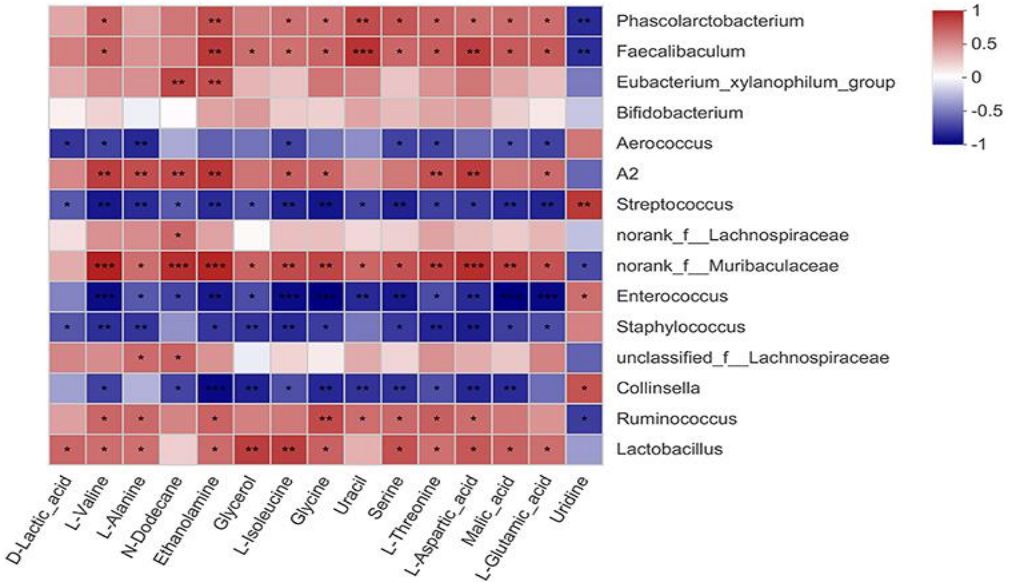

Figure 6. Spearman correlation heatmap depicting relationships between hepatic metabolites and gut bacterial genera. In this representation, red squares indicate positive correlations, blue squares indicate

negative correlations, and white squares denote no significant correlation, with significance levels marked as *p < 0.05, **p < 0.01, and ***p < 0.001.

Our analysis revealed that Streptococcus, Enterococcus, Staphylococcus, and Collinsella were strongly inversely correlated with metabolites such as L-valine, ethanolamine, glycerol, L-isoleucine, glycine, serine, L-threonine, L-aspartic acid, and malic acid, whereas Streptococcus, Enterococcus, and Collinsella showed positive correlations with uridine. In addition, Aerococcus, Streptococcus, and Staphylococcus were negatively associated with D-lactic acid, L-alanine, and L-glutamic acid.

Drug-induced liver injury (DILI) is a potentially severe adverse reaction that may arise unpredictably even with commonly used drugs or predictably at toxic dosages. DILI is now recognized as a major contributor to acute hepatitis and both acute and chronic liver failure [18]. Individuals prone to DILI often display altered hepatic metabolism or impaired excretion of hepatotoxic agents, leading to hepatocyte stress, apoptosis, and immune activation [19]. Alterations in gut microbiota driven by drug metabolites can further influence DILI susceptibility or modulate immune responses via changes in enterohepatic circulation [19]. Established DILI models—including carbon tetrachloride-induced cirrhosis, diethylnitrosamine-induced hepatocellular carcinoma, and acetaminophen-induced hepatotoxicity—demonstrate gut microbiome shifts that play a pivotal role in gut-liver axis pathophysiology [20]. Although MTX is known to induce hepatotoxicity [21], the connection between MTX-induced gut microbiota changes and hepatic metabolic alterations has remained poorly understood.

The Firmicutes phylum represents a major component of gut microbiota. Previous studies indicate that alcoholic liver disease is associated with elevated levels of Firmicutes, Actinobacteriota, Verrucomicrobiota, Proteobacteria, and Desulfobacterota, alongside reduced Bacteroidota and Campilobacterota, whereas interventions such as triadica cochinchinensis honey treatment reduce the Firmicutes/Bacteroidota (F/B) ratio [22]. In mice with acute liver failure, Firmicutes abundance decreases while Bacteroidota increases [23], highlighting that liver injury induced by different methods results in distinct microbiota alterations. In our study, MTX administration led to increased abundances of Firmicutes, Actinobacteriota, and Proteobacteria, whereas Bacteroidota significantly decreased, resulting in an elevated F/B ratio. These findings align with previous observations in Bisphenol A-induced hepatotoxicity, where F/B ratio elevation was linked to liver injury [24]. MTX-challenged mice also exhibited increased liver injury markers (AST and ALT) and H&E staining revealed inflammatory cell infiltration, confirming that MTX simultaneously induces hepatotoxicity and gut microbiota alterations.

At the genus level, Faecalibaculum is characteristic of alcoholic liver injury, whereas norank_f_Muribaculaceae, Lactobacillus, unclassified_f_Lachnospiraceae, and norank_f_Lachnospiraceae have been associated with liver disease [25]. Genera such as Aerococcus, Enterococcus, Collinsella, and Streptococcus are recognized proinflammatory bacteria in various conditions [26, 27], and their increased abundance following MTX exposure suggests potential proinflammatory effects on the liver. This is consistent with prior evidence showing that MTX is metabolized into MTX-polyglutamate (MTX-PG), which accumulates intracellularly, triggering hepatocyte oxidative stress, apoptosis, and inflammation [28]. Liver inflammation promotes excessive reactive oxygen species production, damaging hepatocytes and disrupting enzyme structure and activity via amino acid oxidation [29].

The liver is central to amino acid homeostasis, regulating absorption, utilization, and systemic distribution. Hepatic amino acids serve as substrates for numerous essential metabolic processes [30], and dysregulated amino acid metabolism is linked to hepatotoxic progression [31]. Classic hepatotoxin models—including acetaminophen, bromobenzene, and carbon tetrachloride—demonstrate consistent upregulation in pathways involving glycine, serine, threonine, cysteine, methionine, arginine, proline, glutathione, alanine, aspartate, and glutamate [31]. In our MTX-challenged mice, reductions in Phascolarctobacterium, Faecalibaculum, A2, Streptococcus, norank_f_Muribaculaceae, Ruminococcus, and Lactobacillus correlated positively with amino acid levels, whereas increases in Staphylococcus, Aerococcus, Enterococcus, Collinsella, and Streptococcus correlated negatively. These results suggest that MTX-induced gut microbiota shifts may influence hepatic amino acid metabolism, affecting biosynthetic pathways for valine, leucine, isoleucine, arginine, and metabolic pathways of alanine, aspartate, glutamate, histidine, glycine, serine, and threonine during hepatocyte oxidative stress, apoptosis, or inflammation [29].

tRNA-charged amino acids serve as direct precursors for protein synthesis, and both their abundance and distribution within the aminoacyl-tRNA pool can strongly influence the rate of protein production in tissues [32].

Exposure to fine particulate matter has been reported to induce liver toxicity, with metabolomic analyses revealing significant disruptions in aminoacyl-tRNA biosynthesis and related amino acid metabolic pathways [33]. Similarly, alcohol consumption alters metabolic networks including aminoacyl-tRNA biosynthesis, alanine, aspartate, and glutamate metabolism, as well as energy metabolism [34]. In the present study, MTX-challenged mice exhibited reduced levels of several amino acids in the aminoacyl-tRNA biosynthesis pathway—such as glycine, L-aspartic acid, L-valine, L-alanine, L-isoleucine, L-threonine, and L-glutamic acid—suggesting that MTX impairs protein synthesis. At the genus level, Phascolarctobacterium, Faecalibaculum, A2, Streptococcus, norank_f_Muribaculaceae, Ruminococcus, and Lactobacillus were positively correlated with aminoacyl-tRNA biosynthesis, whereas Staphylococcus, Aerococcus, Enterococcus, Collinsella, and Streptococcus were negatively correlated. Beyond aminoacyl-tRNA, other metabolic pathways affected included biosynthesis of valine, leucine, isoleucine, and arginine; metabolism of alanine, aspartate, glutamate, histidine, beta-alanine, and glycine, serine, and threonine; pantothenate and CoA biosynthesis; and energy metabolism pathways such as glyoxylate and dicarboxylate metabolism. These findings align with COG functional predictions showing that MTX impacts energy production and conversion, as well as amino acid and carbohydrate transport and metabolism.

Glutamic acid, a versatile amino acid present in the CNS and peripheral organs, is a key hepatic metabolite generated through transdeamination of arginine, ornithine, proline, histidine, and glutamine under physiological conditions [35]. Hepatocyte efflux largely determines systemic glutamic acid levels [36]. We hypothesize that MTX-induced liver dysfunction may enhance glutamic acid efflux, disrupting amino acid metabolism and resulting in decreased hepatic levels of glutamic acid and other amino acids. In the gut, both host and microbial metabolism of endogenous (e.g., bile acids, amino acids) and exogenous (dietary or environmental) substrates generates metabolites that travel via the portal vein to the liver, influencing its function [10]. Previous studies have shown altered glutamine metabolism in CCl4-induced acute liver injury, highlighting its role in hepatic stellate cell proliferation and activation [37]. Similarly, LPS-induced liver injury reduces hepatic glutamic acid levels, whereas α-ketoglutarate supplementation restores glutamic acid and supports energy metabolism [38]. In our MTX model, L-glutamic acid was downregulated across multiple amino acid metabolic pathways—including those for alanine, aspartate, glutamate, histidine, glutathione, and arginine biosynthesis—indicating its involvement in hepatocyte proliferation and energy metabolism rather than neurotransmission. Correlation analyses revealed positive associations between L-glutamic acid and Phascolarctobacterium, Faecalibaculum, A2, norank_f_Muribaculaceae, and Lactobacillus, whereas Aerococcus, Streptococcus, Enterococcus, and Staphylococcus were negatively correlated. Consistently, COG function predictions indicated enhanced energy production and amino acid metabolism in the gut microbiota of MTX-treated mice.

Interestingly, metabolomic profiling and COG predictions both implicated CoA-related biological processes in MTX-induced hepatotoxicity. Decreased levels of L-aspartic acid, L-valine, and uracil in MTX-exposed mice suggest disruption of pantothenate and CoA biosynthesis. KEGG pathway analysis (https://www.kegg.jp/pathway/map00770) shows that L-valine and L-aspartic acid can be converted to pantothenate, which is subsequently phosphorylated and metabolized to CoA—a cofactor essential for ~4% of enzymatic reactions in vivo [39]. Compounds such as mangiferin calcium salt have been reported to attenuate type 2 diabetes and NAFLD by modulating pantothenate/CoA biosynthesis, fatty acid metabolism, citric acid cycle intermediates, arginine, and tryptophan metabolism [40]. In our study, MTX increased Streptococcus, Enterococcus, and Collinsella, which negatively correlated with hepatic L-aspartic acid, L-valine, and uracil, suggesting these genera may contribute to altered coenzyme transport and metabolism.

This work provides a preliminary exploration of MTX-induced hepatotoxicity mechanisms, highlighting correlations between differential gut microbiota and hepatic metabolites. Further studies, including fecal microbiota transplantation, are needed to identify key microbial taxa and metabolites responsible for these effects.

Conclusion

MTX exposure induced hepatotoxicity accompanied by significant alterations in gut microbiota and hepatic metabolic pathways. MTX disrupted aminoacyl-tRNA biosynthesis, pantothenate and CoA biosynthesis, amino acid metabolism, energy metabolism, porphyrin and chlorophyll metabolism, and glutathione pathways. Microbiota shifts included increased abundances of Staphylococcus, Enterococcus, Collinsella, Streptococcus, and Aerococcus, and decreased abundances of Lactobacillus, Ruminococcus, norank_f_Muribaculaceae, unclassified_f_Lachnospiraceae, norank_f_Lachnospiraceae, A2, Eubacterium_xylanophilum_group,

Phascolarctobacterium, Bifidobacterium, and Faecalibaculum. Correlation analyses provide insight into the interplay between gut microbiota and hepatic metabolic disturbances, offering a foundation to further investigate mechanisms of MTX-induced hepatotoxicity.

Acknowledgments: None

Conflict of Interest: None

Financial Support: None

Ethics Statement: None

References

1. Koźmiński P, Halik PK, Chesori R, Gniazdowska E. Overview of dual-acting drug methotrexate in different neurological diseases, autoimmune pathologies and cancers. Int J Mol Sci. 2020;21(10):3483. doi:10.3390/ijms21103483
2. Hannoodee M, Mittal M. Methotrexate. In: StatPearls. StatPearls Publishing; 2021.
3. Solomon DH, Glynn RJ, Karlson EW, Lu F, Corrigan C, Colls J, et al. Adverse Effects of Low-Dose Methotrexate: a randomized trial. Ann Intern Med. 2020;172(6):369-80. doi:10.7326/M19-3369. Epub 2020 Feb 18. PMID: 32066146; PMCID: PMC7229518.
4. Bath RK, Brar NK, Forouhar FA, Wu GY. A review of methotrexate-associated hepatotoxicity. J Dig Dis. 2014;15(10):517–24. doi:10.1111/1751-2980.12184
5. Visser K. Van der Heijde D. Risk and management of liver toxicity during methotrexate treatment in rheumatoid and psoriatic arthritis: a systematic review of the literature. DARE. 2009;27(6):1017–25.
6. Yang T, Richards EM, Pepine CJ, Raizada MK. The gut microbiota and the brain–gut–kidney axis in hypertension and chronic kidney disease. Nat Rev Nephrol. 2018;14(7):442–56. doi:10.1038/s41581-018-0018-2
7. Lässiger-Herfurth A, Pontarollo G, Grill A, Reinhardt C. The gut microbiota in cardiovascular disease and arterial thrombosis. Microorganisms. 2019;7(12):691. doi:10.3390/microorganisms7120691
8. Lu L, Chen X, Liu Y, Yu X. Gut microbiota and bone metabolism. FASEB J. 2021;35(7):e21740. doi:10.1096/fj.202100451R
9. Tilg H, Cani PD, Mayer EA. Gut microbiome and liver diseases. Gut. 2016;65(12):2035–44. doi:10.1136/gutjnl-2016-312729
10. Tripathi A, Debelius J, Brenner DA, Karin M, Loomba R, Schnabl B, et al. The gut-liver axis and the intersection with the microbiome. Nat Rev Gastroenterol Hepatol. 2018;15(7):397-411. doi:10.1038/s41575-018-0011-z. Erratum in: Nat Rev Gastroenterol Hepatol. 2018 Dec;15(12):785. doi:10.1038/s41575-018-0031-8. PMID: 29748586; PMCID: PMC6319369.
11. Yi Z , Liu X , Liang L , Wang G , Xiong Z , Zhang H , et al . Antrodin a from antrodia camphorata modulates the gut microbiome and liver metabolome in mice exposed to acute alcohol intake. Food Funct. 2021;12(7):2925-37. doi:10.1039/d0fo03345f. Epub 2021 Mar 15. PMID: 33720247.
12. Roghani M, Kalantari H, Khodayar MJ, Khorsandi L, Kalantar M, Goudarzi M, et al. Alleviation of liver dysfunction, oxidative stress and inflammation underlies the protective effect of ferulic acid in methotrexate-induced hepatotoxicity. Drug Des Devel Ther. 2020;14:1933-41. doi:10.2147/DDDT.S237107. PMID: 32546960; PMCID: PMC7250701.
13. Loke MF, Chua EG, Gan HM, Thulasi K, Wanyiri JW, Thevambiga I, et al. Metabolomics and 16S rRNA sequencing of human colorectal cancers and adjacent mucosa. PLoS One. 2018;13(12):e0208584. doi:10.1371/journal.pone.0208584. PMID: 30576312; PMCID: PMC6303059.
14. Peng W, Huang J, Yang J, Zhang Z, Yu R, Fayyaz S, et al. Integrated 16S rRNA sequencing, metagenomics, and metabolomics to characterize gut microbial composition, function, and fecal metabolic phenotype in non-obese type 2 diabetic goto-kakizaki rats. Front Microbiol. 2020;10:3141. doi:10.3389/fmicb.2019.03141. PMID: 32038574; PMCID: PMC6984327.

15. Liu YJ, Tang B, Wang FC, Tang L, Lei YY, Luo Y, et al. Parthenolide ameliorates colon inflammation through regulating Treg/Th17 balance in a gut microbiota-dependent manner. Theranostics. 2020;10(12):5225-41. doi:10.7150/thno.43716. PMID: 32373209; PMCID: PMC7196297.
16. Forsgård RA, Marrachelli VG, Korpela K, Frias R, Collado MC, Korpela R, et al. Chemotherapy-induced gastrointestinal toxicity is associated with changes in serum and urine metabolome and fecal microbiota in male sprague-dawley rats. Cancer Chemother Pharmacol. 2017;80(2):317-32. doi:10.1007/s00280-017-3364-z. Epub 2017 Jun 23. PMID: 28646338; PMCID: PMC5532424.
17. Freeman-Narrod M, Narrod SA. Chronic toxicity of methotrexate in mice. J Natl Cancer Inst. 1977;58(3):735–41. doi:10.1093/jnci/58.3.735
18. Devarbhavi H, Patil M, Reddy VV, Singh R, Joseph T, Ganga D. Drug-induced acute liver failure in children and adults: results of a single-centre study of 128 patients. Liver Int. 2018;38(7):1322–9. doi:10.1111/liv.13662
19. Andrade RJ, Chalasani N, Björnsson ES, Suzuki A, Kullak-Ublick GA, Watkins PB, et al. Drug-induced liver injury. Nat Rev Dis Primers. 2019;5(1):58. doi:10.1038/s41572-019-0105-0. PMID: 31439850.
20. Dey P. The role of gut microbiome in chemical-induced metabolic and toxicological murine disease models. Life Sci. 2020;258:118172. doi:10.1016/j.lfs.2020.118172
21. Kim J, Kim Y, Choi J, Jung H, Lee K, Kang J, et al. Recapitulation of methotrexate hepatotoxicity with induced pluripotent stem cell-derived hepatocytes from patients with rheumatoid arthritis. Stem Cell Res Ther. 2018;9(1):357. doi:10.1186/s13287-018-1100-1. PMID: 30594247; PMCID: PMC6310944.
22. Luo L, Zhang J, Liu M, Qiu S, Yi S, Yu W, et al. Monofloral triadica cochinchinensis honey polyphenols improve alcohol-induced liver disease by regulating the gut microbiota of mice. Front Immunol. 2021;12:673903. doi:10.3389/fimmu.2021.673903. PMID: 34093575; PMCID: PMC8175904.
23. Zhao J, Liu L, Xin L, Lu Y, Yang X, Hou Y, et al. The protective effects of a modified xiaohua funing decoction against acute liver failure in mice induced by D-Gal and LPS. Evid Based Complement Alternat Med. 2022;2022:6611563. doi:10.1155/2022/6611563. PMID: 35069764; PMCID: PMC8776459.
24. Liu R, Liu B, Tian L, Jiang X, Li X, Cai D, et al. Exposure to bisphenol a caused hepatoxicity and intestinal flora disorder in rats. Int J Mol Sci. 2022;23(14):8042. doi:10.3390/ijms23148042. PMID: 35887390; PMCID: PMC9321671.
25. Zhou J, Zhang N, Zhao L, Mohamed Soliman M, Wu W, Li J, et al. Protective effects of honey-processed astragalus on liver injury and gut microbiota in mice induced by chronic alcohol intake. J Food Qual. 2022;2022(1):5333691.
26. Li BY, Xu XY, Gan RY, Sun QC, Meng JM, Shang A, et al. Targeting gut microbiota for the prevention and management of diabetes mellitus by dietary natural products. Foods. 2019;8(10):440. doi:10.3390/foods8100440. PMID: 31557941; PMCID: PMC6835620.
27. Martínez JE, Vargas A, Pérez-Sánchez T, Encío IJ, Cabello-Olmo M, Barajas M. Human microbiota network: unveiling potential crosstalk between the different microbiota ecosystems and their role in health and disease. Nutrients. 2021;13(9):2905. doi:10.3390/nu13092905
28. Ezhilarasan D. Hepatotoxic potentials of methotrexate: understanding the possible toxicological molecular mechanisms. Toxicology. 2021;458:152840. doi:10.1016/j.tox.2021.152840
29. Zhu R, Wang Y, Zhang L, Guo Q. Oxidative stress and liver disease. Hepatol Res. 2012;42(8):741–9. doi:10.1111/j.1872-034X.2012.00996.x
30. Paulusma CC, Lamers W, Broer S. van de Graaf SF. Amino acid metabolism, transport and signalling in the liver revisited. Biochem Pharmacol. 2022;201:115074. doi:10.1016/j.bcp.2022.115074
31. Pannala VR, Estes SK, Rahim M, Trenary I, O'Brien TP, Shiota C, et al. Toxicant-induced metabolic alterations in lipid and amino acid pathways are predictive of acute liver toxicity in rats. Int J Mol Sci. 2020;21(21):8250. doi:10.3390/ijms21218250. PMID: 33158035; PMCID: PMC7663358.
32. Wolfe RR, Song J, Sun J, Zhang XJ. Total aminoacyl-transfer RNA pool is greater in liver than muscle in rabbits. J Nutr. 2007;137(11):2333–8. doi:10.1093/jn/137.11.2333
33. Shi C, Han X, Mao X, Fan C, Jin M. Metabolic profiling of liver tissues in mice after instillation of fine particulate matter. Sci Total Environ. 2019;696:133974. doi:10.1016/j.scitotenv.2019.133974
34. Fang H, Zhang AH, Sun H, Yu JB, Wang L, Wang XJ. High-throughput metabolomics screen coupled with multivariate statistical analysis identifies therapeutic targets in alcoholic liver disease rats using liquid

chromatography-mass spectrometry. J Chromatogr B. 2019;1109:112–20. doi:10.1016/j.jchromb.2019.01.017

35. Brosnan ME, Brosnan JT. Hepatic glutamate metabolism: a tale of 2 hepatocytes. Am J Clin Nutr. 2009;90(3):857S–61S. doi:10.3945/ajcn.2009.27462Z
36. Pfennig T, Herrmann B, Bauer T, Schömig E, Gründemann D. Benzoic acid and specific 2-oxo acids activate hepatic efflux of glutamate at OAT2. Biochim Biophys Acta. 2013;1828(2):491–8. doi:10.1016/j.bbamem.2012.08.026
37. Li J, Ghazwani M, Liu K, Huang Y, Chang N, Fan J, et al. Regulation of hepatic stellate cell proliferation and activation by glutamine metabolism. PLoS One. 2017;12(8):e0182679. doi:10.1371/journal.pone.0182679. PMID: 28797105; PMCID: PMC5552314.
38. Wang L, Hou Y, Yi D, Li Y, Ding B, Zhu H, et al. Dietary supplementation with glutamate precursor α-ketoglutarate attenuates lipopolysaccharide-induced liver injury in young pigs. Amino Acids. 2015;47(7):1309-18. doi:10.1007/s00726-015-1966-5. Epub 2015 Mar 21. PMID: 25795418.
39. Leonardi R, Zhang YM, Rock CO, Jackowski S. Coenzyme A: back in action. Prog Lipid Res. 2005;44(2–3):125–53. doi:10.1016/j.plipres.2005.04.001
40. Lin H, Teng H, Wu W, Li Y, Lv G, Huang X, et al. Pharmacokinetic and metabolomic analyses of mangiferin calcium salt in rat models of type 2 diabetes and non-alcoholic fatty liver disease. BMC Pharmacol Toxicol. 2020;21(1):59. doi:10.1186/s40360-020-00438-x. PMID: 32762728; PMCID: PMC7409647.